

# VISUALIZING MORPHOGENESIS AND GROWTH BY TEMPORAL INTERPOLATION OF SURFACE-BASED 3D ATLASES

*Chavdar Papazov, Vincent J. Dercksen, Hans Lamecker, Hans-Christian Hege*

Zuse Institute Berlin (ZIB), Takustr. 7, 14195 Berlin, Germany, email: <lastname>@zib.de

## ABSTRACT

Image-based 3D atlases have been proven to be very useful in biological and medical research. They serve as spatial reference systems that enable researchers to integrate experimental data in a spatially coherent way and thus to relate diverse data from different experiments. Typically such atlases consist of tissue-separating surfaces. The next step are 4D atlases that provide insight into temporal development and spatio-temporal relationships. Such atlases are based on time series of 3D images and related 3D models.

We present work on temporal interpolation between such 3D atlases. Due to the morphogenesis of tissues during biological development, the topology of the non-manifold surfaces may vary between subsequent time steps. For animation therefore a smooth morphing between non-manifold surfaces with different topology is needed.

**Index Terms**— Digital anatomy, anatomical atlas, surface reconstruction, temporal interpolation, morphing

## 1. INTRODUCTION

3D models provide considerable assistance for the analysis of anatomy, structure, and function of biological systems. 3D atlases, particularly population-averaged ones [1, 2], enable researchers to integrate experimental data with spatial reference into a common framework – data that were obtained by different experiments on potentially different individuals. After integration these diverse data can be jointly visualized and analyzed – potentially revealing unknown relationships. Such atlases are typically based on histological serial sections or high-resolution tomographic images. To reduce the amount of data to be handled, atlases are mostly surface-based instead of volume-based. The surfaces represent 2D interfaces separating different tissue types.

Similarly, 4D atlases can provide insight into temporal development and spatio-temporal relationships. For instance, in developmental biology gene interactions can be inferred from time-varying 3D gene expression patterns, or gene expressions can be related to differentiation of unspecialized cells and to morphogenesis.

Non-destructive imaging techniques allow for imaging developing individuals, while destructive techniques require

different individuals for the creation of a time series. In the latter case typically much higher resolution is possible, but one is faced with individual variations that ideally should be averaged out by creation of a population average for each time step – before doing temporal interpolation.

In this work we aim at construction of high-resolution 4D atlases of developing organisms that allow the integration of experimental data. We focus on temporal interpolation between discrete time steps of a series of 3D surface-based atlases that have been created from histological serial sections [3]. The tissue-separating surfaces [4] are non-manifold meshes which topology changes with time due to morphogenetical processes during development. Specifically, we discuss how the non-manifold surfaces can be mapped onto each other and how temporal interpolation can be performed, in order to visualize a smoothly developing organism.

## 2. RELATED WORK

Much work has been done in the field of 3D reconstruction of biological objects from image data. Creating such models usually involves a number of processing steps: 2D registration (in case the input data is a stack of 2D histological slices), segmentation and surface reconstruction. The 2D registration is usually achieved by a rigid transformation, optionally followed by an elastic deformation step [5, 6]. Segmentation is a very problem-specific task. Different solution strategies exist, e.g. methods based on pure image-processing, model-based methods (e.g. [7]), and machine-learning methods (see [8] for an overview). Unlike boundary-based segmentation algorithms, which usually already result in a surface separating different tissues, voxel-based methods require an additional surface reconstruction step [9]. The final surface is potentially non-manifold. An example of such a reconstruction pipeline is described in [3].

Several types of algorithms have been presented in the past, which compute a smooth transition between two objects: a start and a target object (see [10] for an overview). Distance field interpolation (DFI) based methods achieve this by interpolating distance fields defined for the start and target objects [11]. Such methods are able to handle topologically different start and target objects. The shape of the intermediate objects is given by the zero level set of the interpolated

distance field, which is difficult to control and may result in undesired shapes. To reduce such deformations, [12] propose to interpolate a combination of the distance field and a user-defined non-linear transformation, which maps corresponding points on each object onto each other. DFI-based methods are however not able to handle non-manifold objects. This also holds for methods based on other types of implicit functions, e.g. [13]. Surface-based morphing methods [14] usually require a bijective mapping to be defined between start and target object. The transition is then computed by interpolating the position of corresponding points. These methods however require the surface to be homeomorphic to a sphere or a disk. This restraint can be relaxed by dividing a non-manifold surface into disk-like patches [4]. None of these methods is however able to interpolate between topologically different objects. [15] proposes a method which enable this, but is not very intuitive and cannot handle non-manifold surfaces.

### 3. MORPHING BETWEEN TOPOLOGICALLY DIFFERENT NON-MANIFOLD MESHES

We base our method on [4] and extend it to be able to handle certain topological changes. The basic idea is to 1) decompose both surfaces into disk-like patches, 2) assign to each patch of the start object one or more corresponding patches on the target object and 3) morph between corresponding patches. By cloning patches, we create topologically equivalent surfaces and we can use the morphing technique from [4] to transform one surface into the other.

#### 3.1. Correspondence Establishment

*Patchwise correspondence.* We let the user decompose both input meshes in a number of patches. This is done interactively by drawing the borders (separation lines) of the patches with the mouse directly on the surface. In order to compute a global bijection between the meshes (cf. Sect. 3.3) every patch must be homeomorphic to a disc. This is however not a restriction to the morphing algorithm, because every finite (manifold and non-manifold) surface can be decomposed in a finite number of disc-like patches.

If the input meshes are homeomorphic to each other, the user must decompose them in the same number of patches and define a bijective correspondence (e.g. as a table) between them. Furthermore every patch of one mesh must have the same neighbours as its counterpart of the other mesh.

In the case of topologically different input meshes, we do not have a bijective correspondence: there are patches of one surface that must be assigned to several patches of the other surface.

*Correspondence between the patch borders.* For making the input meshes topologically equivalent a correspondence — which is in general not bijective — between their patch

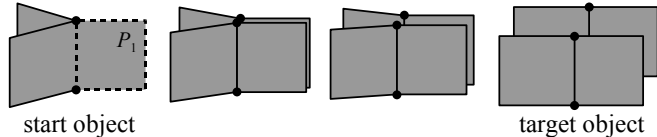


**Fig. 1.** Copying patch  $P_1$ , the dashed borders and both branching points in order to make start and target object topologically equivalent.

borders is also needed. In most cases a border is uniquely described by its adjacent patches. If the correspondence cannot be computed automatically, the user must define it.

*Correspondence between the branching points.* Given the correspondence between the borders, every branching point of one mesh can be automatically assigned to its counterpart(s) of the other mesh. This is possible because a branching point is uniquely defined as a starting or end point of a border. The underlying assumption is that corresponding borders have the same direction.

#### 3.2. Topology modification

After the correspondences have been established, we make the objects topologically equivalent by cloning patches, borders and branching points of the input meshes in the following way. A patch of one surface, which is assigned to  $n \geq 1$  patches of the other surface will be copied  $n - 1$  times so that the copies and the original patch will have exactly one counterpart in the other surface. We do the same with the borders and branching points. Figure 1 illustrates this situation for two artificial surfaces. After applying these operations to every patch, border and branching point of both input meshes, they will be homeomorphic to each other.

Notice that the copy operations described above do not modify the geometry of the meshes. This means that the topology modifications are achieved without a visible effect: the parts of the meshes are just copied without altering their position in space.

#### 3.3. Computation of a global bijective mapping

The problem of establishing a global bijective mapping between two topologically equivalent surfaces is solved by computing a bijective mapping between every two corresponding patches and combining the mappings to form one global bijection. To have a smooth transition between the meshes, this bijection must be overall continuous. First, continuity at the borders and the branching points is ensured. These border maps constrain the common parameterization of the interior of the patches, resulting in the global bijectivity. For more details, we refer to [4].

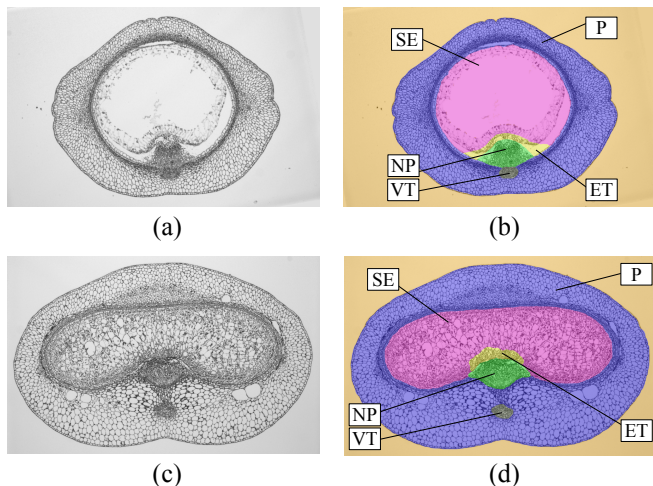


**Fig. 2.** (a) and (c) Cross section of a barley grain made at the fourth and seventh day after flowering. (b) and (d) Segmented version of the image on the left. Legend: ET – endosperm transfer cells, NP – nucellar projection, P – pericarp, SE – starchy endosperm, VT – vascular tissue.

### 3.4. Connectivity merging

We now modify both meshes such that they have the same connectivity. For each pair of corresponding patches, the patch with the smallest number of triangles (say  $P1$ ) is re-triangulated. This is done by mapping the triangles of the other mesh onto  $P1$  using the bijective mapping computed in the previous subsection. This results in two meshes with identical connectivity and corresponding vertices.

### 3.5. Interpolation

The final morph is produced by a linear interpolation between corresponding vertices of both meshes. Such an interpolation method does not guarantee an intersection-free morphing sequence. Our tests have shown, that this is not a problem for geometrically similar surfaces.

## 4. RESULTS AND DISCUSSION

### 4.1. Results

Fig. 2 shows cross-sections through the middle part of two barley grains. The images in the upper row are taken on the fourth day after flowering (4DAF) and those in the lower row on the seventh day (7DAF). From these images surface models have been created. Notice that between these time steps, the nucellar projection and the vascular tissue (NP and VT in Figures 2(b) and 2(d)) are separated. The same happens with the endosperm transfer cells (ET) and the pericarp (P). These changes cause the topological differences between the 4DAF mesh (cf. Fig. 3 for  $t=0.0$ ) and the 7DAF mesh ( $t=1.0$ ).

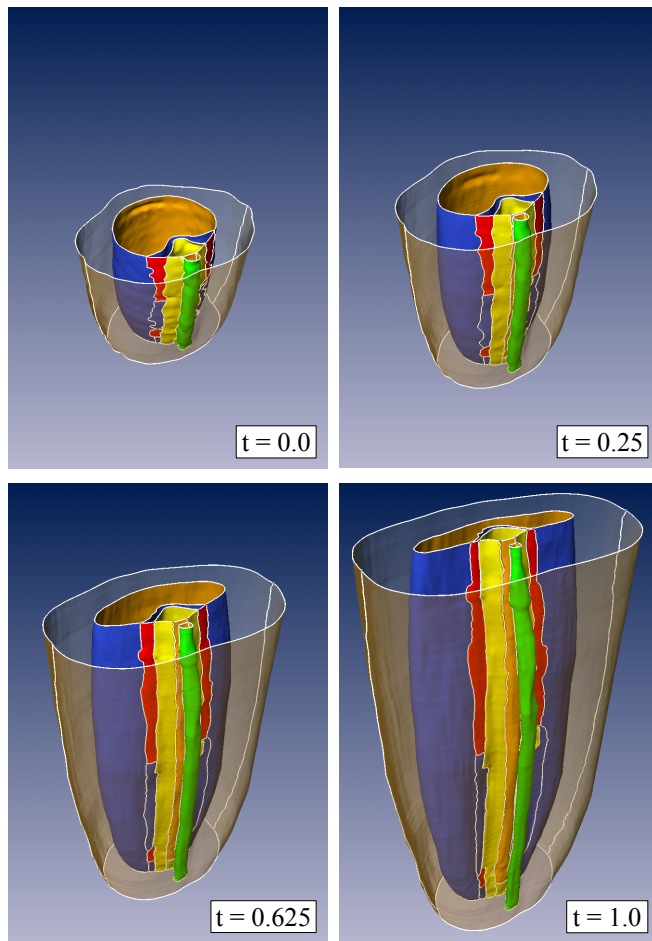


**Fig. 3.** A morph between two topologically different non-manifold meshes. The mesh at  $t = 0.0$  is reconstructed from an image stack of a barley grain four days after flowering. The surface at  $t = 1.0$  represents a barley grain seven days after flowering.

Fig. 3 shows four frames from the morph sequence between the non-manifold meshes of the two barley grains, computed with our method. To emphasize the increasing size of the grain, the camera position was fixed.

The cross-sections in Fig. 4 focus on the topological evolution of the mesh during the morphogenesis.

### 4.2. Discussion

We presented a morphing algorithm capable of morphing between two topologically different non-manifold meshes. The method was successfully tested on two surface models of a real biological system: developing barley grains.

There are however some limitations. Topological changes caused by surface parts, that emerge out of nothing cannot be computed by the presented algorithm. This is due to the fact, that the input meshes are being modified by copying their

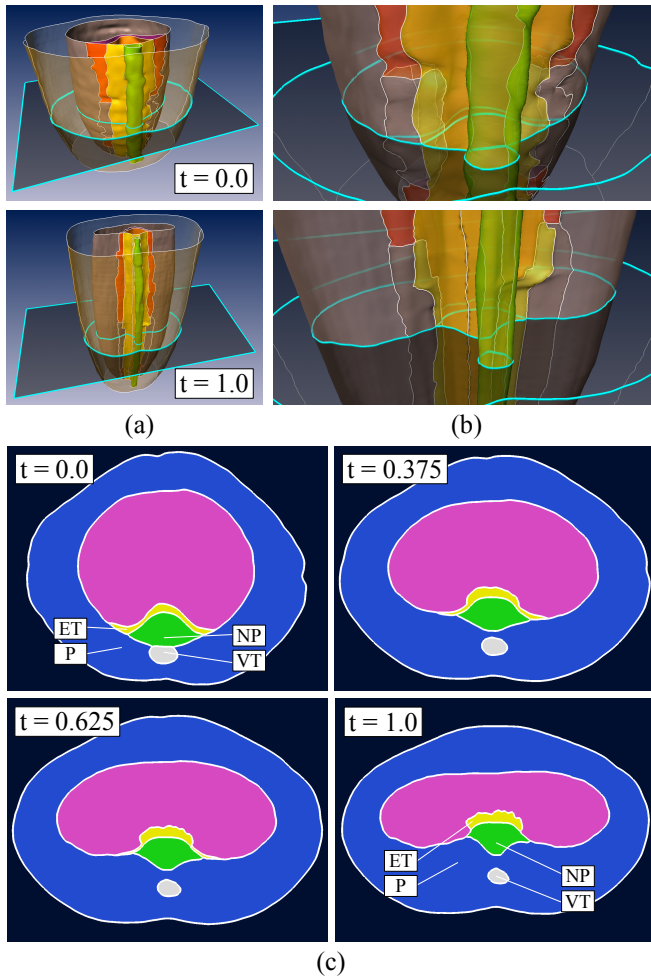


**Fig. 4.** The same surfaces as in Fig. 3 shown in different colours and from another view point. (a) The input meshes at the beginning ( $t = 0.0$ ) and at the end ( $t = 1.0$ ) of the morph. (b) Zoom at the intersection line between the meshes and a plane. (c) Four intersections between the evolving mesh and a plane. Notice the change in the shape of the endosperm transfer cells (ET) and the separation between the nucellar projection (NP) and the vascular tissue (VT).

patches until they are topologically equivalent. This cannot be done in the case of appearance or disappearance, because there is only one input mesh.

We thank Dr. Winfriede Weschke and Diana Weier of the Leibniz Institute of Plant Genetics and Crop Plant Research, Germany, for providing the barley data. V.J. Dercksen is supported by BMBF grant 0312706B. H. Lamecker is supported by the DFG research center MATHEON.

## 5. REFERENCES

- [1] R. Brandt et al., “A three-dimensional average-shape atlas of the honeybee brain and its applications,” *J. Comp.*

*Neurol.*, vol. 492(1), pp. 1–19, 2005.

- [2] A. Kuss et al., “Pipeline for the creation of surface-based averaged brain atlases,” in *Proc. of WSCG 2007*, Plzen, Czech Republic, Jan. 2007, vol. 1, pp. 17–24.
- [3] V.J. Dercksen et al., “Towards automatic generation of 3d models of biological objects based on serial sections,” in *Visualization in Medicine and Life Sciences*. 2008, pp. 3–25, Springer.
- [4] M. Zöckler et al., “Fast and intuitive generation of geometric shape transitions,” *The Visual Computer*, vol. 16, no. 5, pp. 241–253, 2000.
- [5] T. Ju et al., “3D volume reconstruction of a mouse brain from histological sections using warp filtering,” *J. Neurosci. Methods*, vol. 156, pp. 84–100, 2006.
- [6] S. Wirtz et al., “Super-fast elastic registration of histologic images of a whole rat brain for three-dimensional reconstruction,” in *Proc. SPIE, Medical Imaging*, 2004.
- [7] D. Kainmüller et al., “Shape constrained automatic segmentation of the liver based on a heuristic intensity model,” *Proc. MICCAI Workshop 3D Segmentation in the Clinic: A Grand Challenge*, pp. 109–116, 2007.
- [8] J. Rogowska, “Overview and fundamentals of medical image segmentation,” *Handbook of medical imaging*, pp. 69–85, 2000.
- [9] H.C. Hege et al., “A Generalized Marching Cubes Algorithm Based on Non-Binary Classifications,” Tech. Rep. Preprint SC-97-05, Zuse Institute Berlin, 1997.
- [10] M. Alexa, “Recent advances in mesh morphing,” *Computer Graphics Forum*, vol. 21, no. 2, pp. 173–196, 2002.
- [11] D. Levin, “Multidimensional reconstruction by set-valued approximation,” *IMA J. Numerical Analysis*, vol. 6, pp. 173–184, 1986.
- [12] D. Cohen-Or et al., “Three-dimensional distance field metamorphosis,” *ACM Transactions on Graphics (TOG)*, vol. 17, no. 2, pp. 116–141, 1998.
- [13] G. Turk and J. F. O’Brien, “Shape transformation using variational implicit functions,” in *Proceedings of SIGGRAPH 99*, 1999, pp. 335–342.
- [14] A. Shapiro, “Polyhedron realization for shape transformation,” *The Visual Computer*, vol. 14, no. 8/9, pp. 429–444, 1998.
- [15] D. DeCarlo and J. Gallier, “Topological evolution of surfaces,” *Graphics Interface*, pp. 194–203, 1996.